Grain boundary dynamics in stripe phases of nonpotential systems

Zhi-Feng Huang
Department of Physics and Astronomy, Wayne State University, Detroit, Michigan 48201, USA
and McGill Institute for Advanced Materials, and Department of Physics, McGill University, Montreal, QC H3A 2T8, Canada

Jorge Viñals
McGill Institute for Advanced Materials, and Department of Physics, McGill University, Montreal, QC H3A 2T8, Canada
(Received 11 December 2006; published 7 May 2007)

We describe numerical solutions of two nonpotential models of pattern formation in nonequilibrium systems to address the motion and decay of grain boundaries separating domains of stripe configurations of different orientations. We first address wave-number selection because of the boundary, and possible decay modes when the periodicity of the stripe phases is different from the selected wave number for a stationary boundary. We discuss several decay modes including long wavelength undulations of the moving boundary, as well as the formation of localized defects and their subsequent motion. We find three different regimes as a function of the distance to the stripe phase threshold and initial wave number, and then correlate these findings with domain morphology during domain coarsening in a large aspect ratio configuration.

DOI: 10.1103/PhysRevE.75.056202 PACS number(s): 89.75.Kd, 05.45.−a, 47.54.−r, 47.20.Bp

I. INTRODUCTION

A stripe configuration is a particular example of a modulated configuration that exhibits structural periodicity along only one spatial direction. In thermodynamic equilibrium, these phases have been widely observed in a variety of systems [1], including, for example, microphase separated block copolymers [2]. Outside of equilibrium, stripe patterns are also widespread, including Rayleigh-Bénard convection in fluids [3,4], or electroconvection in nematic liquid crystals [5,6]. When the lateral size of the system of interest is large compared with the wavelength of the modulation (large aspect ratio limit), a stripe configuration in either class of systems is usually characterized by a transient multidomain and defected configuration with only local order. Domain coarsening is believed to be controlled by the motion of existing topological defects in the configuration such as grain boundaries, dislocations, and disclinations. In this paper, we focus on nonpotential (or no variational) model systems and investigate the processes of defect formation and motion near grain boundaries, and show that there exist several regimes in parameter space that are characterized by qualitatively different coarsening behavior.

A major topic of interest in domain coarsening of stripe patterns is the growth law for the characteristic linear scale of the configuration. This has been addressed both in theoretical studies [7–11] and in experiments in nematics [6,12] and block copolymers [13]. Although our focus here is on isotropic pattern forming systems, we mention existing research in anisotropic systems such as the oblique roll pattern in electroconvection in nematics [5,6,12], with its specific defect configurations [14] and some similarities with isotropic systems [15]. The characteristic length scale $R(t)$ is expected to obey a power law growth in time, $R(t) \sim t^x$, with a value of the coarsening exponent x which ranges from 1/5 to 1/2 in the studies to date. The actual value appears to depend on ϵ (the dimensionless distance from the onset of the stripe phase) [10,16], thermal noise [7], and the type of length scale under study [8,11]. Also, domain morphologies, as well as the value of x, have been found to be different in potential systems (in which the evolution is solely driven by minimization of a potential) than in the nonpotential case [8]. Numerical studies of the Swift-Hohenberg model of Rayleigh-Bénard convection (a potential system) suggest that $x=1/3$ in the limit $\epsilon \ll 1$ as a result of grain boundary motion [9]. As ϵ increases, the value of x is seen to decrease from 1/3, a fact that was argued to be a manifestation of defect pinning [16]. On the other hand, the generalized Swift-Hohenberg model has been studied as an example of a nonpotential model [8], and it has been shown that the evolution of stripe patterns is asymptotically dominated by the motion of isolated dislocations. Furthermore, recent results from a direct solution of the Boussinesq equations in a Rayleigh-Bénard configuration suggest that multiple length scales should be introduced in the case of nonpotential systems [11].

Despite a significant body of research on domain coarsening of modulated patterns, the mechanisms responsible for the observed properties and the values of the coarsening exponents, especially for nonpotential systems, are not yet understood. We report in this paper our analysis of the relation between the selected wave number at grain boundaries and the critical wave number, and consequences on both early time defect formation and asymptotic coarsening. Our starting point is a planar 90° grain boundary separating two stripe domains of mutually perpendicular orientations, as shown in Fig. 1. We determine the selected wave vector for a stationary boundary configuration $\mathbf{q}^s$ in two different nonpotential models, and show that for other wave numbers the mode of decay of the configuration can be classified according to its wave number and the dimensionless distance from threshold ϵ. For small ϵ, an initially planar grain boundary separating two domains, one of which at least has $\mathbf{q} \neq \mathbf{q}^s$, is seen to propagate, either as a planar front, or by developing long wavelength undulations, depending on the value of $\mathbf{q}$. For larger values of ϵ we find that the grain boundary configuration decays through the formation of disclinations around the boundary and their subsequent motion. We then correlate our

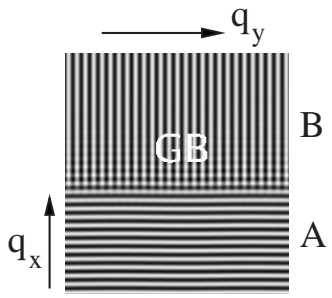

FIG. 1. A 90° tilt grain boundary (GB) configuration of a stripe phase, with wave numbers q_x and q_y for two domains A and B of mutually perpendicular stripe orientations.

findings with the observed domain coarsening morphology of configurations obtained from initially uniform but unstable states. The rationale for the comparison is the observation that in an extended system an early time transient configuration following the decay of an unstable state will comprise a distribution of locally ordered domains with a wave number approximately equal to the critical wave number for instability q_0, but with different orientations. Depending on whether q_0 is close to q^s or not, the resulting boundaries will be locally close to being stationary, or quickly decay leaving behind different types of defects. The ensuing domain coarsening is shown to be different depending on the (near) stability of grain boundaries that spontaneously form in the early stages following the decay of the initially unstable configuration.

Our study is based on a numerical solution of two different nonpotential extensions of the Swift-Hohenberg model of Rayleigh-Bénard convection [3], as described in Sec. II. One of them is made nonpotential on account of the specific choice of nonlinearity, whereas the other allows for mean flows representing the effect of vertical vorticity encountered in Rayleigh-Bénard convection in small Prandtl number fluids [17]. They are described in Secs. III and IV, respectively. Although wave-number selection for a stationary grain boundary is different in both models, similar properties concerning grain boundary motion and decay have been found. They correlate with two types of domain coarsening behavior, either grain boundary dominated or disclination and/or dislocation dominated, as deduced from the results on grain boundary decay that will be discussed in Sec. V.

II. NONPOTENTIAL MODEL EQUATIONS

The model systems we have investigated are two-dimensional generalized Swift-Hohenberg equations which have been used as a phenomenological description of stripe patterns [3,17]:

$$\partial_t \psi + \mathbf{U}\cdot\boldsymbol{\nabla}\psi = \epsilon\psi - (\nabla^2 + q_0^2)^2\psi - g\psi^3 + 3(1-g)|\nabla\psi|^2\nabla^2\psi, \tag{1}$$

where $\psi(x,y,t)$ is a dimensionless real order parameter field, and the control parameter ϵ is the distance from the threshold for instability of the solution $\psi=0$ (at $\epsilon=0$). The wave number q_0 ($q_0=1$ in the dimensionless units that we are using) is the critical wave number for instability. An advection term with a drift velocity $\mathbf{U}(x,y,t)=(U_x,U_y)$ has been added to Eq. (1) to introduce mean flow effects resulting from the coupling to vertical vorticity in the fluid [17,18]. The velocity $\mathbf{U}(x,y,t)$ is given in terms of the vorticity potential $\zeta(x,y,t)$,

$$\mathbf{U} = \boldsymbol{\nabla}\times(\zeta\hat{\mathbf{z}}) = (\partial_y\zeta, -\partial_x\zeta), \tag{2}$$

which satisfies

$$[\partial_t - \sigma(\nabla^2 - c^2)]\nabla^2\zeta = g_m[\boldsymbol{\nabla}(\nabla^2\psi)\times\boldsymbol{\nabla}\psi]\cdot\hat{\mathbf{z}}, \tag{3}$$

with σ being the Prandtl number of the fluid, c^2 introduced to phenomenologically model the effect of no slip boundary conditions at the top and bottom plates of the convection cell [18], and the coupling parameter g_m chosen to be a decreasing function of the Prandtl number. Following Ref. [17], a Gaussian filtering operator F_γ is introduced on the right-hand side of Eq. (3) to reduce high wave vector contributions to the vertical vorticity. In Fourier space, F_γ acts by multiplying the Fourier transform of the filtered function by a factor

$$\hat{F}_{\gamma_q} = e^{-\gamma^2 q^2}, \tag{4}$$

where $q^2=q_x^2+q_y^2$, with wave-vector components q_x and q_y, and γ represents the filtering radius.

Different types of model equations for describing stripe patterns have been included in Eqs. (1)–(3), depending on the values of g and g_m. For $g=1$ and $g_m=0$ (so that $\mathbf{U}=0$), the nonlinearity in the model is given by the cubic term ψ^3 only, leading to the original Swift-Hohenberg equation [19], which is a potential model. A nonpotential model without mean flows follows from $g=g_m=0$ (referred to as model 1 in this paper), which includes a nonlinear term of the form $|\nabla\psi|^2\nabla^2\psi$. For $g=1$ and $g_m\neq 0$ (and hence $\mathbf{U}\neq 0$), we obtain the Swift-Hohenberg model supplemented by mean flows, also a nonpotential system (model 2).

The initial configuration considered in the first part of our study is a 90° tilt boundary separating two stripe domains, as shown in Fig. 1. A stationary state is known to exist [20] if unique values of the wave numbers q_x (for the stripes parallel to the grain boundary in domain A) and q_y (for the stripes perpendicular to the boundary in domain B) are selected in both domains. For the original Swift-Hohenberg model, these wave numbers are $q_x=q_y=q_0$. In our numerical study, we consider instead a symmetric pair of grain boundaries along the x direction so that periodic boundary conditions can be adopted. The pseudospectral algorithm described in Ref. [21] has been used to numerically solve the model equations, with a time step $\Delta t=0.2$ and a grid spacing $\Delta x=\Delta y=\lambda_0/8$ (i.e., 8 grid points per stripe wavelength $\lambda_0=2\pi/q_0$). Most of our results shown below correspond to a system size 512×512 grid nodes, with spot checks with larger sizes (2048×2048) to verify our results.

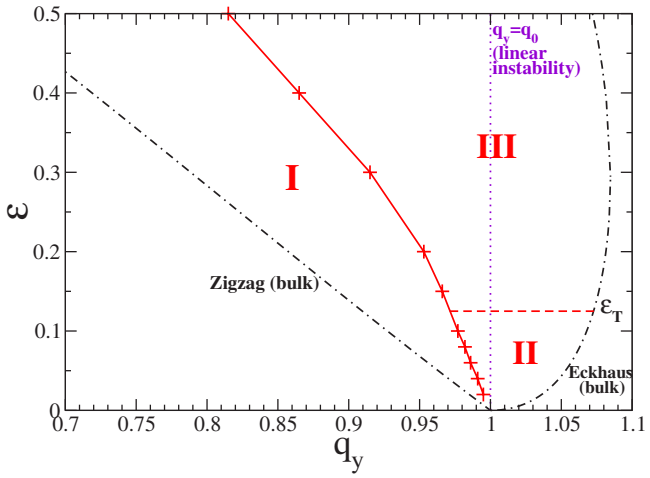

FIG. 2. (Color online) Stability diagram for the nonpotential model 1 as a function of ϵ and q_y (the wave number of the stripes perpendicular to the grain boundary). The plus symbols correspond to the unique wave vector $(q_x, q_y) = [q_x^s = q_0 - \epsilon/(2q_0^3), q_y^s]$ for a stationary grain boundary configuration. Also shown (as dot-dashed lines) are stability boundaries for bulk Eckhaus and zigzag instabilities. Three regimes for grain boundary decay are indicated, and also the critical wave number q_0 for linear instability.

III. WAVE-VECTOR SELECTION AND GRAIN BOUNDARY DECAY—MODEL 1

A. Wave-number selection

Model 1 includes the nonlinear term $|\nabla\psi|^2\nabla^2\psi$ but does not have mean flow. The selected wave numbers (q_x^s and q_y^s) for a stationary grain boundary configuration have been already calculated by Tesauro and Cross [20]. Their analysis of the appropriate amplitude equations for this case yields

$$q_x^s = q_0 - \frac{\epsilon}{2q_0^3} \tag{5}$$

up to order ϵ for the selected wave number in domain A, and $q_y^s = q_0$ up to order $\epsilon^{3/4}$ for domain B. They also conducted a limited numerical study of this model to suggest that $q_y^s \simeq q_0 - 0.12\epsilon$ (although this result is based on calculations involving only two different values of ϵ).

We have numerically calculated the selected wave numbers for the same configuration but with much larger system sizes and longer integration times. Our results for q_x^s are in agreement with Eq. (4), but the calculated values of q_y^s are different from those of previous studies, as presented in Figs. 2 and 3. The deviation of q_y^s from the critical wave number q_0 is seen to obey two different power laws in ϵ. For small $\epsilon < \epsilon_0$, with ϵ_0 around 0.2, we find (Fig. 3)

$$q_y^s \simeq q_0 - 0.23\epsilon, \tag{6}$$

while for larger ϵ we obtain,

$$q_y^s \simeq q_0 - 0.525\epsilon^{3/2}. \tag{7}$$

Note that although both results differ from the numerical calculations of Ref. [20], they are not inconsistent with an analysis based on amplitude equations.

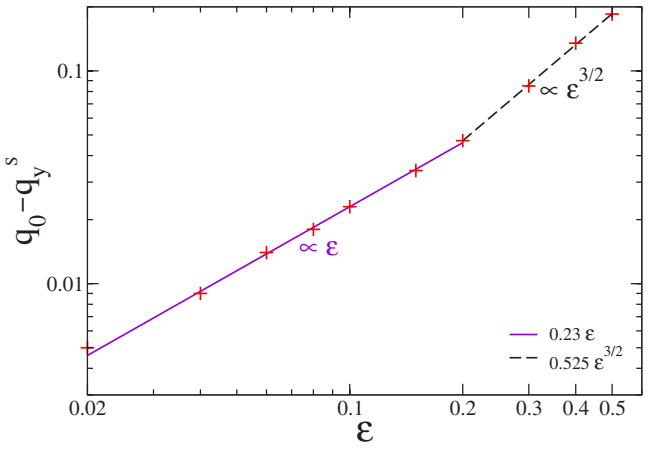

FIG. 3. (Color online) Wave number q_y^s for a stationary grain boundary (model 1) as a function of ϵ. The figure shows two different types of dependency on ϵ: $q_0 - q_y^s \propto \epsilon$ (for small ϵ) and $\propto \epsilon^{3/2}$ (for larger ϵ).

B. Decay of the grain boundary configuration

Given the results of Eqs. (4)–(6), and also our numerical results in Fig. 2, it is clear that the wave number selected by a grain boundary is different from q_0, the most unstable mode near onset. Thus, the locally dominant wave number during the early stages of coarsening could be significantly different from (q_x^s, q_y^s), and therefore it appears to be of value to study the decay of grain boundaries under those conditions. Of course, grain boundaries would not be fully formed at those early stages, but we hope that studying unstable trajectories away from well-defined grain boundary configurations will illustrate differences in observed morphologies between potential and nonpotential models.

We start by noting that in the configuration which we consider there is no phase conservation in the x direction. Hence if $q_x \neq q_x^s$ is chosen initially, the bulk wave number of domain A can readjust to q_x^s through lamella formation or destruction near the boundary [20]. We will not consider this case. More complicated phenomena can occur for $q_y \neq q_y^s$, and this is the focus of our study: In the calculations that follow we always keep $q_x = q_x^s$ in domain A, while we explore a range of values of q_y in domain B.

As indicated in Fig. 2, we find that our results can be qualitatively classified according to the values of q_y and ϵ. This leads to the existence of three parameter regimes distinguished by $q_y < q_y^s$ and $q_y > q_y^s$, and in the latter case by the value of ϵ with a threshold ϵ_T separating two qualitatively different regimes of grain boundary decay, as detailed below.

In regime I defined by $q_y < q_y^s$, the two grain boundaries move from domain A towards domain B until they merge. Both boundaries remain approximately planar during the process. Such a motion is found for all the values of ϵ investigated, with a particular example of $\epsilon = 0.3$ and $q_y = 0.85$ shown in Fig. 4(a).

On the other hand, a longitudinal distortion of the stripes in domain B around the grain boundary region is observed if $q_y > q_y^s$. In addition, the evolution following the appearance of the initial distortion is qualitatively different depending on

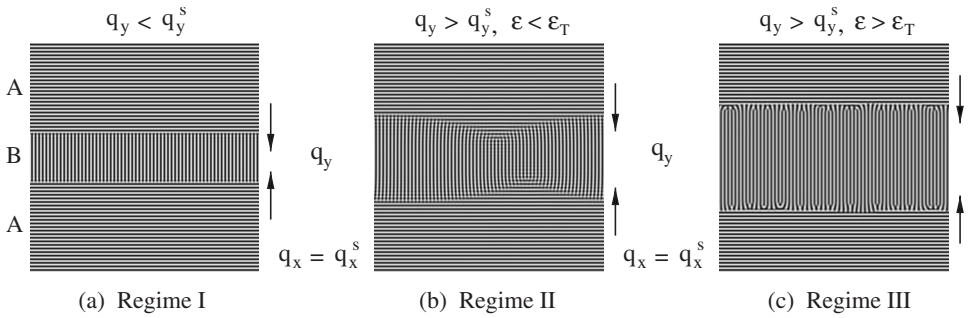

FIG. 4. Grain boundary decay in the three regimes shown in Fig. 2 for model 1, with $q_x=q_x^s$. The direction of boundary motion is indicated by arrows. (a) Regime I: $q_y<q_y^s$ for all ϵ; the example shown here corresponds to $q_y=0.85$, $\epsilon=0.3$ and at $t=1200$. (b) Regime II: $q_y>q_y^s$ and $\epsilon<\epsilon_T$; we have chosen $q_y=q_0=1$, $\epsilon=0.04$, and $t=10^4$. (c) Regime III: $q_y>q_y^s$ and $\epsilon>\epsilon_T$; the configuration shown here corresponds to $q_y=q_0=1$, $\epsilon=0.5$, and $t=100$.

the value of ϵ. In regime II of Fig. 2 with $\epsilon<\epsilon_T$ (where the value of ϵ_T is around 0.1 to 0.2 as estimated from our numerical solutions), long-range undulations of diffuse grain boundaries are observed, as shown in Fig. 4(b). The stripes of domain B are curved around the boundaries, the latter moving towards each other at the expense of domain B until they finally merge. Despite the undulations, the grain boundary configuration in regime II is preserved during the process. In regime III on the other hand, the boundary is sharp, and the longitudinal distortion leads to the formation of convex disclinations in the boundary region [Fig. 4(c) for $\epsilon>\epsilon_T$]. The boundary itself also moves towards the bulk of domain B as indicated by the arrows in the figure, resulting again in the eventual disappearance of the grain boundary configuration.

The longitudinal distortions that we observe in both regimes, including the formation of an array of disclinations in regime III, are due to wave number mismatch between the initial value q_y and the stationary value $q_y^s<q_y$. In regime II [Figs. 4(b)], periodic longitudinal modulation of stripes B appears, reminiscent of an Eckhaus distortion that promotes wave-number reduction. Since the velocity of the boundary depends on the local wave number of stripes B ahead of it, a modulation of the boundary position also results from this wave-number variation. In regime III, on the other hand, the boundary is sharp, and cross rolls, dislocations, and disclinations form at the edges of domain B leading also to wave-number reduction. The bulk of domains A and B, however, remain largely unperturbed.

In order to verify that this spontaneous distortion originates in the boundary region, we have studied the decay of the configuration shown in Fig. 5(a) in which slow transverse modulations of wave number $Q\ll q_x$ and phase magnitude δ have been added to the initial condition of $q_x=q_x^s$ in domain A. In this case, $q_y=q_y^s$ in the bulk of domain B but not at the grain boundaries. For large ϵ (regime III), the grain boundaries decay through the formation of disclinations, as shown in Fig. 5(b). The same decay was shown in Fig. 4(c) corresponding to the case $q_y\neq q_y^s$ in the whole domain B.

A similar analysis can be carried out in regime II (small ϵ), with the same conclusion. We note, however, an interesting aspect of the decay as compared to potential models. The grain boundary moves from the modulated domain A towards the undistorted domain B, exactly the opposite of what is expected for a potential model given our choice of wave numbers. With the consideration that wave numbers q_x and q_y in the bulk of both domains are equal to the stationary values q_x^s and q_y^s of the corresponding potential model, the extra energy that is stored in the modulated stripes in domain A would lead to boundary motion in the opposite direction [9].

IV. WAVE-VECTOR SELECTION AND GRAIN BOUNDARY DECAY—MODEL 2

The second nonpotential model studied, as described in Sec. II, includes the so-called mean flows. They are known to have a significant effect on the stability of a stripe configuration [17], on defect dynamics [22,23], and allow the appearance of spiral defect chaos [24]. We consider here the decay of the grain boundary configuration studied above. We have chosen model parameter values that are typical for fluid systems in Eqs. (1)–(3): $\sigma=1$, $c^2=2$, $g_m=10$, and $\gamma=\lambda_0/2$ for filtering.

We have first verified numerically that the unique wave numbers for a stationary grain boundary are $q_x^s=q_y^s=q_0$, the same as in the potential Swift-Hohenberg model. This result follows from the observation that the lowest-order contribution of mean flow to the amplitude equations of a grain boundary is $\mathcal{O}(\epsilon^{5/4})$ [22].

The known stability diagram of a stripe configuration is similar to that shown in Fig. 2 for model 1, except that q_y^s

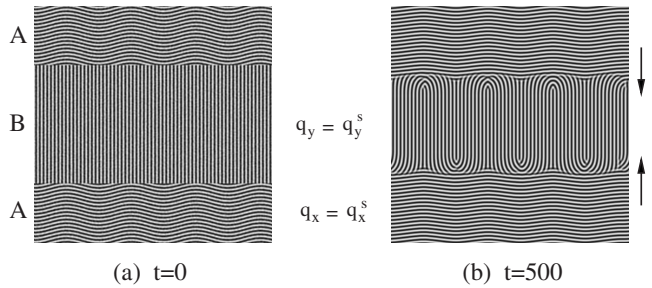

FIG. 5. Grain boundary decay (for model 1) due to a slow transverse modulation of domain A in an initial stationary configuration (with $q_x=q_x^s$ and $q_y=q_y^s$), with $\epsilon=0.5$, the modulation wave number $Q=q_x/16$, and the magnitude of the phase modulation $\delta=\lambda_0$.

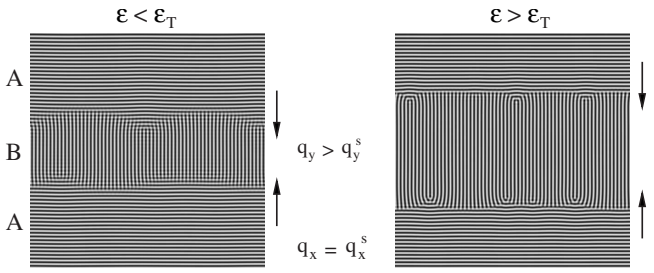

FIG. 6. Grain boundary decay for model 2 as a result of mean flows, with $g_m=10$, $\sigma=1$, $c^2=2$, and $q_x=q_x^s=q_0$. (a) Regime II: $q_y>q_y^s$ and $\epsilon<\epsilon_T$; the parameters used in this case are $q_y=1.02$, $\epsilon=0.04$, and $t=4000$. (b) Regime III: $q_y>q_y^s$ and $\epsilon>\epsilon_T$; the configuration shown corresponds to $q_y=1.02$, $\epsilon=0.3$, and $t=600$.

$=q_0=1$, and the type and detailed location of the stability boundaries are different (e.g., the Eckhaus boundary in Fig. 2 should be replaced by the skewed-varicose boundary [17]). In terms of our study of the decay of a grain boundary, we also find in this model three different regimes which are qualitatively similar to those of model 1. Rigid motion of the grain boundary is observed when $q_y<q_y^s$ for all ϵ, while a longitudinal distortion of the stripes in domain B appears when $q_y>q_y^s$. We can also qualitatively distinguish between regimes II ($\epsilon<\epsilon_T$) and III ($\epsilon>\epsilon_T$), with two typical examples given in Fig. 6.

As was the case in model 1, we observe long wavelength distortions of the stripes in domain B in regime II [Fig. 6(a)], whereas regime III leads to the formation and subsequent motion of disclinations, and with them, the decay of the grain boundary configuration [Fig. 6(b)]. Disclinations also appear as a result of local deviation of wave numbers from q_y^s in the grain boundary region. This has been verified by adding slow transverse modulations on A stripes while keeping $\mathbf{q}=\mathbf{q}^s$ in the bulk of both domains, with results that are qualitatively similar to those of Fig. 5.

The driving force behind the appearance of longitudinal distortions, and with them either long wavelength undulations or the formation of disclinations, is again local wavenumber reduction around the boundary. This is analogous to what is observed in model 1, and has been already described in detail in Sec. III B. However, once the undulations have been formed or the defects nucleated, mean flows are effective in their subsequent motion. This can be seen from the spatial distribution of the vorticity potential ζ, or the corresponding drift velocity $\mathbf{U}$ obtained in our numerical solutions. In particular, we note that mean flows play a key role in the motion of disclinations in regime III, a regime in which disclinations become pinned in their absence ($g_m \to 0$).

V. DISCUSSION AND CONCLUSIONS

The results described on the decay of a grain boundary configuration in nonpotential models shows the existence of a range of parameters in which the decay leads to the formation of defects (mostly dislocations and disclinations) in the boundary region. This occurs for a configuration in which the stripes parallel to the boundary plane have the selected wave number $q_x=q_x^s$, whereas the stripes perpendicular to the boundary are under slight compression $q_y>q_y^s$. Also, defects are only seen above a certain threshold $\epsilon>\epsilon_T$. Below the threshold, undulations and motion of the boundary follow, but no additional defects are produced.

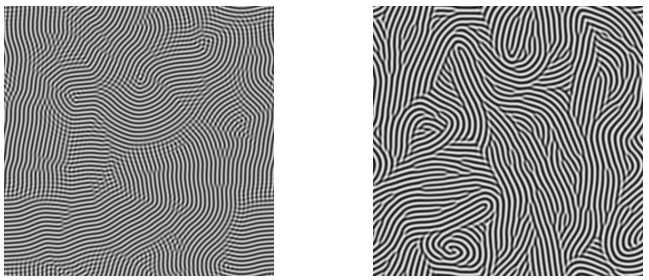

FIG. 7. Multidomain configurations for model 1 showing different qualitative coarsening behavior for (a) $\epsilon<\epsilon_T$ (with $\epsilon=0.04$ and at $t=1000$) and (b) $\epsilon>\epsilon_T$ (with $\epsilon=0.5$ and at $t=500$).

These results can help interpret qualitative features of domain coarsening behavior, both in potential and nonpotential models. In the case of nonpotential model 1 (with a $|\nabla\psi|^2\nabla^2\psi$ nonlinearity), the stationary wave numbers q_x^s and q_y^s are different from q_0, the most unstable wave number [see Eqs. (4)–(6) and Fig. 2]. Following the decay of an initially disordered configuration ($\psi=0$), and the appearance of locally ordered domains with wave number approximately equal to q_0, grain boundaries would be expected to decay according to the mechanism described for regimes II and III depending on the value of ϵ. Whether coarsening takes place in the regime in which the decay of boundaries leads to the formation of dislocations and disclinations (regime III), or to their motion (regime II), one might anticipate qualitatively different late time domain coarsening. Figure 7 shows the results of a numerical integration of model 1 from an initial random configuration of ψ for two particular values of ϵ, both below and above ϵ_T. For $\epsilon<\epsilon_T$ [Fig. 7(a)], grain boundaries are visible in the late time configuration as expected from the results shown in Fig. 4(b). Qualitatively different behavior is observed for $\epsilon>\epsilon_T$ due to the early stage formation of dislocations or disclinations around the emerging grain boundaries. Our results in this case are shown in Fig. 7(b), with the resulting disclination and/or dislocation dominated morphology. These results are consistent with earlier observations in Ref. [8], and more recent research on the Boussinesq equations in Ref. [11]. The average wave number of the evolving configuration changes from q_0 at early times following the instability, towards a long time value that is closer to the stationary wave number of isolated dislocations. One anticipates that domain coarsening will be qualitatively different from the case of small ϵ, as suggested by the results of Ref. [8] showing a complex scaling behavior at large ϵ.

In the case of model 2 which includes a coupling to mean flows, the selected wave numbers q_x^s and q_y^s approximately coincide with the critical wave number for instability q_0, and therefore the effects described above will be weaker, but not

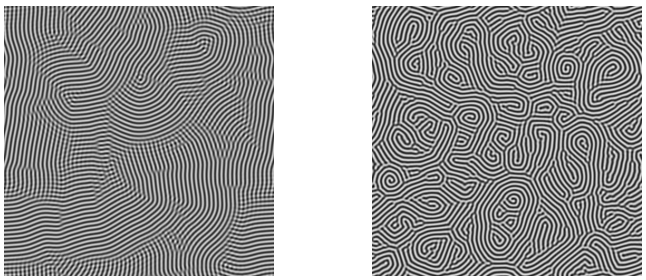

(a) $\varepsilon < \varepsilon_T$ (b) $\varepsilon > \varepsilon_T$

FIG. 8. Multidomain configurations of stripe phase in nonpotential model 2 (with mean flows), for (a) $\epsilon < \epsilon_T$ ($\epsilon=0.04$ and $t=1000$) and (b) $\epsilon > \epsilon_T$ ($\epsilon=0.5$ and $t=1000$). Other parameters are the same as those in Fig. 6: $g_m=10$, $\sigma=1$, and $c^2=2$.

completely absent as local deviations between the stripe wave number and the selected wave number still occur in regions in which the stripes are curved. Near threshold ($\epsilon < \epsilon_T$), the morphology of a transient stripe configuration is shown in Fig. 8(a) obtained by numerical solution of the governing equations from a random initial condition. A stripe pattern qualitatively similar to both model 1 and the potential Swift-Hohenberg model is found, characterized by differently oriented domains separated by 90° grain boundaries. On the other hand, when ϵ exceeds a certain threshold ϵ_T, grain boundaries are expected to be absent as described in Sec. IV. The subsequent evolution of the system in this case is much more complicated resulting in persistent dynamics (spiral defect chaos [24]), as shown in Fig. 8(b).

Unlike experiments addressing the motion of a front separating a domain of spiral defect chaos convection and a domain of parallel rolls (see Ref. [4], and references therein), the configurations shown in Fig. 6(b) does not lead to the formation of spiral defect chaos. The domain of parallel rolls (domain A in the figure) invades the other one with disclinations (domain B), and the latter domain disappears before we are able to observe any chaotic motion. There are, however, several differences with respect to the experiments. First, the rolls of domain A can readjust their wave number at the boundaries so that it remains at its stationary value. This is in contrast with the experiments in which rolls were uniformly compressed towards the skewed-varicose instability boundary. Second, and as a consequence, local wave number changes in the domain boundary region do not lead to states that are unstable against transverse perturbations, and hence this mechanism cannot be invoked to explain front motion in our case. All we have been able to do in this work is to correlate the region in wave number and ϵ that leads to the formation of localized disclinations from a boundary separating two domains of rolls perpendicular to each other with the onset of spiral defect chaos from a uniform, random initial configuration.

In both nonpotential cases discussed in this paper we would expect qualitatively different domain coarsening behavior depending on the interplay between the critical wave number for instability and the selected wave number at a grain boundary. This is in contrast with the potential Swift-Hohenberg model in which grain boundary dynamics is known to dominate for small ϵ until pinning effects at finite ϵ effectively arrest motion [10,16]. In this model, the selected wave numbers for a stationary grain boundary configuration are $q_x^s=q_y^s=q_0$ [20], with $q=q_0$ also marking the stability boundary of the bulk zigzag instability. Therefore, a diagram analogous to that of Fig. 2 would only have regimes II and III characterizing grain boundary motion. In both $q_y > q_y^s$, longitudinal distortions around the boundary can also be identified as a result of local wave-number reduction towards $q_y^s=q_0$. In analogy with the nonpotential cases, in regime II (with $\epsilon < \epsilon_T$) diffuse boundaries with long-range undulations of B stripes are observed. For $\epsilon > \epsilon_T$, the formation of convex disclinations around the boundary can also be seen in our numerical calculations. However, despite their emergence these disclinations become pinned along with the grain boundaries, mainly due to the nonadiabatic effects arising from the coupling between fast scales of base stripe patterns and slow scales of the associated envelopes [16]. This results in a glassy configuration with very slow dynamics. Interestingly, this pinning phenomenon is only observed in the potential Swift-Hohenberg model, but not in the two nonpotential models studied here. In this latter case, grain boundaries quickly decay at large ϵ leaving behind a domain morphology dominated by disclinations and dislocations [Fig. 7(b)], or spiral defects [Fig. 8(b)].

In summary, we have studied wave-number selection, motion, and decay of grain boundaries in a stripe configuration based on a pair of two-dimensional generalized Swift-Hohenberg model equations that are nonpotential in nature. Three different regimes of grain boundary dynamics have been identified, with longitudinal distortions emerging around the grain boundary and manifesting themselves either as long-range undulations of the moving boundary or in the formation and subsequent motion of defects such as convex disclinations. When an extended system is taken from an initial state below threshold to $\epsilon > 0$, the initial decay of the unstable state will lead to the formation of locally ordered domains with a distribution of orientations. Domain interfaces will form in accordance with the analysis given above, and therefore qualitative differences in domain coarsening are expected depending on the value of ϵ.

ACKNOWLEDGMENTS

This research has been supported by the National Science Foundation under Grant No. DMR-0100903, and by NSERC Canada.

[1] M. Seul and D. Andelman, Science **267**, 476 (1995).
[2] F. S. Bates and G. H. Fredrickson, Phys. Today **52**, 32 (1999).
[3] M. C. Cross and P. C. Hohenberg, Rev. Mod. Phys. **65**, 851 (1993).
[4] E. Bodenschatz, W. Pesch, and G. Ahlers, Annu. Rev. Fluid Mech. **32**, 709 (2000).
[5] R. Ribotta, A. Joets, and L. Lei, Phys. Rev. Lett. **56**, 1595 (1986).
[6] L. Purvis and M. Dennin, Phys. Rev. Lett. **86**, 5898 (2001).
[7] K. R. Elder, J. Viñals, and M. Grant, Phys. Rev. Lett. **68**, 3024 (1992).
[8] M. C. Cross and D. I. Meiron, Phys. Rev. Lett. **75**, 2152 (1995).
[9] D. Boyer and J. Viñals, Phys. Rev. E **63**, 061704 (2001).
[10] D. Boyer and J. Viñals, Phys. Rev. E **64**, 050101(R) (2001).
[11] M. R. Paul, K.-H. Chiam, M. C. Cross, and P. F. Fischer, Phys. Rev. Lett. **93**, 064503 (2004).
[12] C. Kamaga, F. Ibrahim, and M. Dennin, Phys. Rev. E **69**, 066213 (2004).
[13] C. Harrison, D. A. Adamson, Z. Cheng, J. M. Sebastian, S. Sethuraman, D. A. Huse, R. A. Register, and P. M. Chaikin, Science **290**, 1558 (2000).
[14] H. Zhao and L. Kramer, Phys. Rev. E **62**, 5092 (2000).
[15] D. Boyer, Phys. Rev. E **69**, 066111 (2004).
[16] D. Boyer and J. Viñals, Phys. Rev. E **65**, 046119 (2002).
[17] H. S. Greenside and M. C. Cross, Phys. Rev. A **31**, 2492 (1985).
[18] P. Manneville, J. Phys. (Paris) **44**, 759 (1983).
[19] J. Swift and P. C. Hohenberg, Phys. Rev. A **15**, 319 (1977).
[20] G. Tesauro and M. C. Cross, Philos. Mag. A **56**, 703 (1987).
[21] M. C. Cross, D. I. Meiron, and Y. Tu, Chaos **4**, 607 (1994).
[22] G. Tesauro and M. C. Cross, Phys. Rev. A **34**, 1363 (1986).
[23] T. Walter, W. Pesch, and E. Bodenschatz, Chaos **14**, 933 (2004).
[24] H.-W. Xi, J. D. Gunton, and J. Viñals, Phys. Rev. Lett. **71**, 2030 (1993).